Supporting Information

Jadi and Sejnowski 10.1073/pnas.1405300111

SI Methods

Stochastic Spiking Neurons. Individual neurons in the model were treated as coupled, continuous-time, two-state (active and quiescent) Markov processes (1). The active state represents a neuron firing an action potential and its accompanying refractory period, whereas the quiescent state represents a neuron at rest. The transition probability for the i^{th} neuron to decay from active to quiescent state in time dt was $P_i(active \rightarrow quiescent) = \alpha_i dt$, where α represented the decay rate of the active state of the neuron. Parameter α_i set the upper bound on firing rate of the stochastically spiking neuron, similar to refractory period. The transition probability for the i^{th} neuron to spike, that is, to change from quiescent to active state, was $P_i(quiescent \rightarrow active) = \beta_i G(S_i(t))dt$. This caused the firing probability to be a function of the input, with β_i as its peak value. Parameter S_i was the total synaptic input to neuron i, given as $S_i(t) = N_i(t) + I_i(t)$, where N_i was the net input from other neurons in the local network and I_i was the net external input to the neuron. The network input was $N_i(t) = \sum_j w_{ij} A_j(t)$, where w_{ij} are the weights of the synapses. The activity variable $A_j(t)$ was set to one (1) if the j^{th} neuron was active at time t and zero otherwise. The model neurons had no intrinsic capacity to oscillate because the interspike interval was the sum of two independent exponential random variables with parameters α_i and $\beta_i G(S_i)$, respectively. Excitatory (E) and inhibitory (I) neurons in the network were differentiated on the basis of two parameters of the model neurons: $\alpha_E = 0.04\ \text{ms}^{-1}$, $\alpha_I = 0.12\ \text{ms}^{-1}$ and $\beta_E = .4$, $\beta_I = .8$. The response function of transition probability of individual neurons was defined by the function described in *Methods*. The results in the main text were qualitatively unchanged when we changed the probability function to different nonlinearities as well as slopes. We used the Gillespie algorithm (2) [software implementation based on Wallace et al. (1)], an event-driven method of simulation, for all simulations of the master equation.

Conditions for Oscillations. Strong E-E and E-I connections were used for population-level oscillations to emerge in a model such as ours whose individual neurons show little oscillation in their spiking activity or in their rates. Comparable oscillation mechanisms have been studied elsewhere (1, 3, 4) to explain other aspects of narrowband oscillations such as the wide distribution of spiking phase with respect to the ongoing oscillations, cycle skipping, and low firing rates of individual neurons (5) in the cortex, characteristics that are robustly demonstrates by our model (Fig. S1).

SI Data Analysis

Spectrogram. The spectrograms (Fig. 5) were generated using the methods of wavelet transforms using a Morlet basis function. The wavelet transform coefficients were calculated using the Wavelet Toolbox in the MATLAB software. The frequency-to-scale mapping in the spectrogram was done by calibration via best frequency-to-scale match for a sine wave signal.

Spike Probability. The cyclo-histogram of spike probability as a function of gamma phase was calculated using simulation data of all 1,000 neurons in our network, at the peak frequency of gamma as calculated from the average power spectrum. The probability distribution was calculated with 20 s of simulation data over 50 phase bins.

SI Notes

Experimental findings (6) suggest that the center frequency of gamma oscillations increases with the contrast of a visual stimulus covering the classical receptive field (center) as well as extraclassical receptive field (surround). At the same time, experiments with increasing size of a visual stimulus suggest that the frequency decreases with the strength of surround suppression (7), a phenomenon of reduction in spikes rate by visual stimulation of surround. The strength of surround suppression also depends on the contrast of stimulus in the surround. This experimental evidence can be combined to propose a simple relationship for gamma-range frequency as a function of stimulus contrast as summarized in Eq. **S1**, where F and G are monotonically increasing functions of contrast. The center frequency of detectable gamma oscillations at the lowest contrast is the baseline frequency:

$$freq_{gamma} = freq_{baseline} + F(contrast_{center}) - G(contrast_{surround}). \quad \textbf{[S1]}$$

This predicts that increasing contrast of visual stimulus in the receptive field center makes the oscillations faster (6) and that of the receptive field surround makes them slower, as shown in the results in Fig. 4. Because uniformly covarying the contrast of center and surround results in a net increase in the gamma-range oscillation frequency (6), Eq. **S1** has to satisfy the condition in Eq. **S2**:

$$F(contrast) > G(contrast). \quad \textbf{[S2]}$$

Eqs. **S1** and **S2** predict that modulating the contrast of center and surround visual stimulus will have no effect on the gamma-range frequency if they are covaried such that they satisfy Eq. **S3**:

$$F(contrast_{center}) = G(contrast_{surround}). \quad \textbf{[S3]}$$

To get an intuition for the condition described by Eq. **S3**, we can derive it for a simple choice of functions F and G, as in Eq. **S4**, which coarsely approximates the experimental data and model predictions:

$$freq_{gamma} = freq_{baseline} + \overbrace{A \times contrast_{center}}^{F} - \overbrace{B \times contrast_{surround}}^{G}$$

where

$$A > B \ \text{ (see Eq. S2)}. \quad \textbf{[S4]}$$

The analysis predicts that frequency of gamma-band oscillations will remain unchanged if Eq. **S3** is satisfied. Substituting for F and G, the oscillation frequency will be unchanged if the contrasts of the visual stimulus in receptive field center and surround are covaried at a ratio less than 1 (one) (Eqs. **S4** and **S5**):

$$\frac{contrast_{center}}{contrast_{surround}} = \frac{B}{A}. \quad \textbf{[S5]}$$

The precise estimation of this ratio will require combining existing experimental data and that obtained from experiments suggested in Fig. 4.

1. Wallace E, Benayoun M, van Drongelen W, Cowan JD (2011) Emergent oscillations in networks of stochastic spiking neurons. *PLoS ONE* 6(5):e14804.
2. Gillespie DT (1977) Exact stochastic simulation of coupled chemical reactions. *J Phys Chem* 81(25):2340–2361.
3. Wilson HR, Cowan JD (1972) Excitatory and inhibitory interactions in localized populations of model neurons. *Biophys J* 12(1):1–24.
4. Brunel N, Wang X-J (2003) What determines the frequency of fast network oscillations with irregular neural discharges? I. Synaptic dynamics and excitation-inhibition balance. *J Neurophysiol* 90(1):415–430.
5. Pesaran B, Pezaris JS, Sahani M, Mitra PP, Andersen RA (2002) Temporal structure in neuronal activity during working memory in macaque parietal cortex. *Nat Neurosci* 5(8):805–811.
6. Ray S, Maunsell JHR (2010) Differences in gamma frequencies across visual cortex restrict their possible use in computation. *Neuron* 67(5):885–896.
7. Gieselmann MA, Thiele A (2008) Comparison of spatial integration and surround suppression characteristics in spiking activity and the local field potential in macaque V1. *Eur J Neurosci* 28(3):447–459.

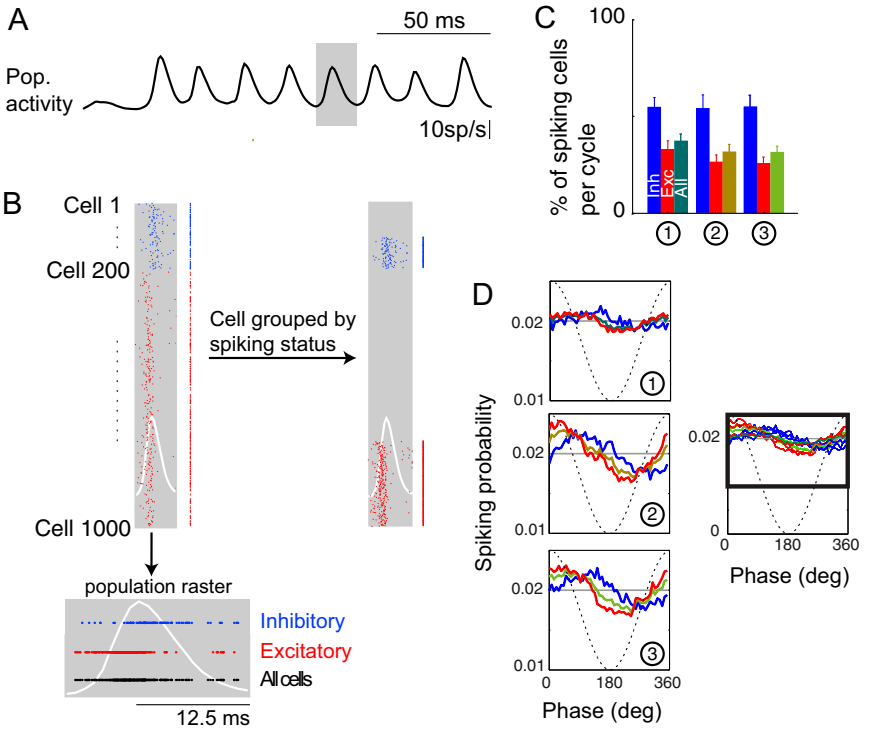

Fig. S1. Single neuron activity in the oscillating network. (*A*) An example trace of oscillations in population activity (total spikes per time bin) in the network. (*B*) Spike raster in a cycle of oscillating population activity in the trial shown in *A* (gray highlighted part of the trace). The population activity (white trace) is shown for reference. Gray rectangle in top left panel shows activity of all cells arranged by their IDs. Blue dots indicate activity of inhibitory cells and red dots indicated activity of excitatory cells. A time-collapsed version is shown on the side to illustrate active (colored dot) vs. nonactive (white space) cells in the particular oscillation cycle. Gray rectangle in top right panel shows the same raster with spiking cells grouped together to illustrate the fraction of cells active in an oscillation cycle. Gray rectangle in bottom left shows the same raster as multiunit activity for excitatory (red), inhibitory (blue), and whole population (green). (*C*) Fraction of neuronal population firing per oscillation cycle of the mean activity (red, excitatory; blue, inhibitory; green palate, all neurons). These statistics were calculated from 20 s of simulation data for each scenario shown in Fig. 1*B*. (*D*) Spike phase probability of all (green), excitatory (red), and inhibitory (blue) neurons as a function of the phase of ongoing oscillations. This was calculated with respect to the oscillation at peak frequency in the power spectrum of population activity, indicated by the dotted sinusoid. Solid gray line indicates a scenario when spikes occur at any phase of the ongoing oscillations with equal probability. Panel on the right shows the probabilities for all cases shown in Fig. 1*B*. Panels on the left zoom into the highlighted timescale in the panel on the right for each scenario in Fig. 1*B*.

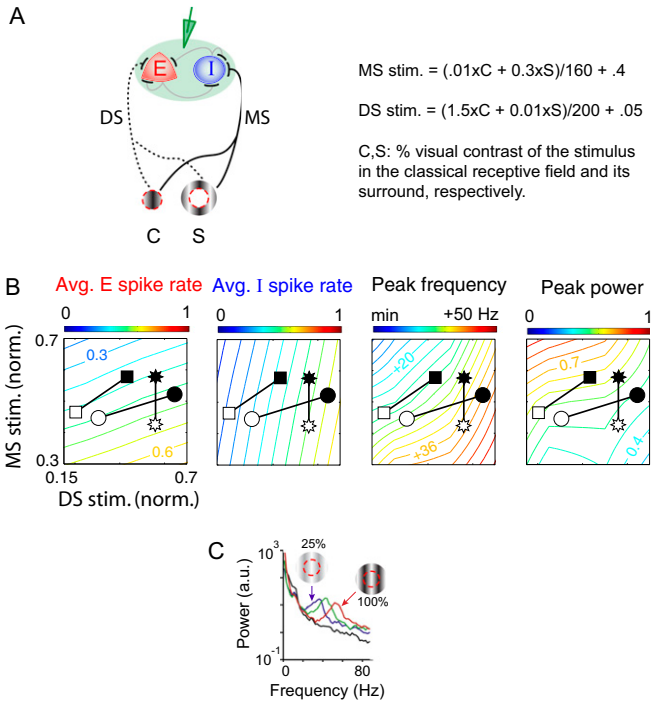

Fig. S2. Contrast dependence of gamma in visual cortex in model and experiments. (*A*) Linear translation formulae used to map the contrast of visual input described in Fig. 4*B* to stimulation of monosynaptic (MS) and disynaptic (DS) pathways in the model local visual cortical circuit. (*B*) Average spiking and oscillatory activity of neuronal population for the three scenarios of visual stimulation (indicated by three symbols) described in Fig. 4*B*. (*C*) Stimulus-induced gamma-range oscillations in the primary visual cortex increase their frequency with increasing contrast of the classical receptive field and its surround [adapted from Ray and Maunsell (6)]. The figure shows power in the local field potential signal at different frequencies.

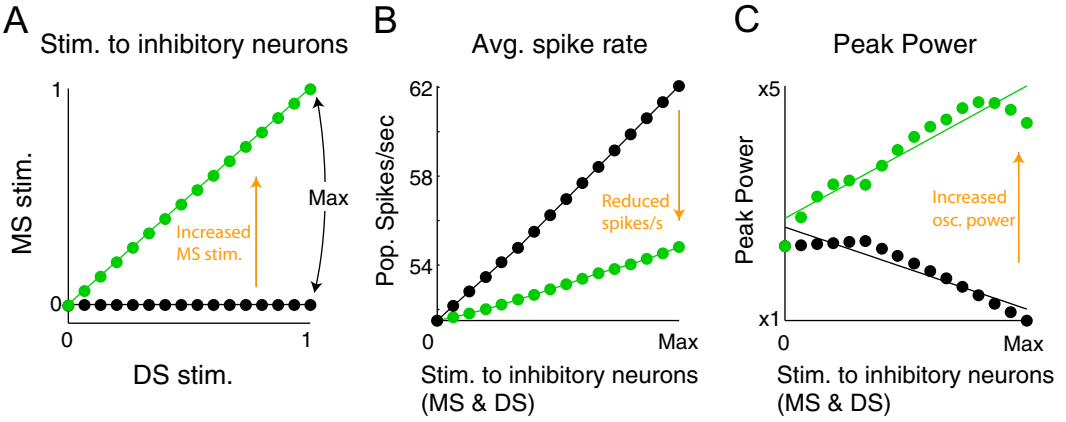

Fig. S3. Divisive normalization of spiking activity in the model network co-occurs with increased narrowband power. (*A*) An example of input scenarios leading to divisive normalization of the output spiking: increasing DS stimulation with weak/zero (black) and strong (green) stimulation to MS pathway in the model. The normalized stimulation units on the axes correspond to the ones shown in the main text Figs. 1 and 2. (*B*) Mean spike rates of the population in response to the two input scenarios shown in *A*. When the stimulation of MS pathway is increased with the DS pathway (green), the resulting population spike rates are scaled divisively compared with the scenario of weak MS stimulation (black). The data show average of 10 trials for each stimulation scenario. The *x* axis indicates combined increasing strength of stimulation (from 0 to maximum) to both MS and DS pathways for the scenarios described in *A*. **(C)** Power of peak narrowband oscillations in the population in response to the two input scenarios shown in *A*. When the stimulation of MS pathway is increased with the DS pathway (green), the resulting oscillation power is increased compared with the corresponding scenario of weak MS stimulation (black). The data show average of 10 trials for each stimulation scenario. The *x* axis indicates combined increasing strength of stimulation (from 0 to maximum) to both MS and DS pathways for the scenarios described in *A*.